Cell Reports

Article

HIV Antibody Fc N-Linked Glycosylation Is Associated with Viral Rebound

Graphical Abstract

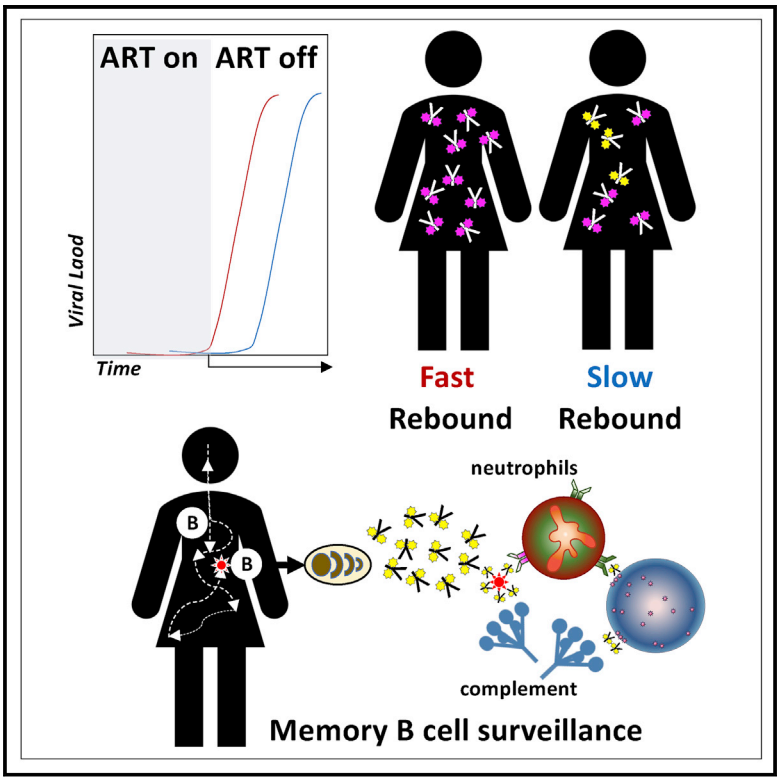

Authors

Rasmus Offersen, Wen-Han Yu, Eileen P. Scully, ..., Dan H. Barouch, Ole S. Søgaard, Galit Alter

Correspondence

galter@mgh.harvard.edu

In Brief

Using systems serology, Offersen et al. demonstrate that HIV-specific antibody Fc N-galactosylation is associated with longer time to viral rebound after discontinuation of antiretroviral treatment across three independent HIV cohorts. Thus, virus-specific antibody glycosylation may represent a promising, simply measured marker to track viral reservoir reactivation.

Highlights

- HIV-specific antibody glycosylation is associated with time to viral rebound
- The glycosylation profile is also linked with altered functional antibody activity
- Plasmablast expansions occur in tandem with antibody glycan shifts
- B cell responses may act as biosensors for viral reactivation and control in tissues

Offersen et al., 2020, Cell Reports *33*, 108502
December 15, 2020
https://doi.org/10.1016/j.celrep.2020.108502

CellPress

Cell Reports

CellPress
OPEN ACCESS

Article

HIV Antibody Fc N-Linked Glycosylation Is Associated with Viral Rebound

Rasmus Offersen,[1,2,3,11] Wen-Han Yu,[1,4,11] Eileen P. Scully,[1,5] Boris Julg,[1] Zelda Euler,[1] Saheli Sadanand,[1] Dario Garcia-Dominguez,[1] Lu Zheng,[6] Thomas A. Rasmussen,[2] Madeleine F. Jennewein,[1] Caitlyn Linde,[1] Jessica Sassic,[1] Giuseppe Lofano,[1] Selena Vigano,[1] Kathryn E. Stephenson,[7] Stephanie Fischinger,[1] Todd J. Suscovich,[1] Mathias Lichterfeld,[8] Douglas Lauffenburger,[4] Erik S. Rosenberg,[9] Todd Allen,[1] Marcus Altfeld,[10] Richelle C. Charles,[9] Lars Østergaard,[2,3] Martin Tolstrup,[2,3] Dan H. Barouch,[1,7] Ole S. Søgaard,[2,3] and Galit Alter[1,12,*]

[1]Ragon Institute of MGH, MIT, and Harvard, Cambridge, MA 02139, USA
[2]Department of Infectious Diseases, Aarhus University Hospital, Aarhus 8000, Denmark
[3]Department of Clinical Medicine, Aarhus University, Aarhus 8000, Denmark
[4]Department of Biological Engineering, Massachusetts Institute of Technology, Cambridge, MA 02139, USA
[5]Department of Medicine, Division of Infectious Diseases, Johns Hopkins University School of Medicine, Baltimore, MD 21205, USA
[6]Department of Biostatistics, Harvard T.H. Chan School of Public Health, Boston, MA 02115, USA
[7]Center for Virology and Vaccine Research, Beth Israel Deaconess Medical Center, Boston, MA 02115, USA
[8]Division of Infectious Disease, Brigham and Women's Hospital, Boston, MA 02115, USA
[9]Division of Infectious Disease, Massachusetts General Hospital, Boston, MA 02114, USA
[10]Heinrich Pette Institute, Leibniz Institute for Experimental Virology, 20251 Hamburg, Germany
[11]These authors contributed equally
[12]Lead Contact
*Correspondence: galter@mgh.harvard.edu
https://doi.org/10.1016/j.celrep.2020.108502

SUMMARY

Changes in antibody glycosylation are linked to inflammation across several diseases. Alterations in bulk antibody galactosylation can predict rheumatic flares, act as a sensor for immune activation, predict gastric cancer relapse, track with biological age, shift with vaccination, change with HIV reservoir size on therapy, and decrease in HIV and HCV infections. However, whether changes in antibody Fc biology also track with reservoir rebound time remains unclear. The identification of a biomarker that could forecast viral rebound time could significantly accelerate the downselection and iterative improvement of promising HIV viral eradication strategies. Using a comprehensive antibody Fc-profiling approach, the level of HIV-specific antibody Fc N-galactosylation is significantly associated with time to rebound after treatment discontinuation across three independent cohorts. Thus virus-specific antibody glycosylation may represent a promising, simply measured marker to track reservoir reactivation.

INTRODUCTION

The major obstacle for HIV "cure" strategies is the latent reservoir. Early during infection, HIV exploits numerous mechanisms of immune evasion to establish this latent reservoir, resulting in lifelong infection (Finzi et al., 1999). Several novel approaches have been proposed to reactivate, or "shock," the latent virus in quiescent infected cells to drive viral transcription and render them visible to the immune system, permitting rapid destruction and viral eradication. Histone deacetylase (HDAC) inhibitors have been used in recent clinical trials to activate latent viral genomes, although only marginal effects on the viral reservoir size have been shown (Archin et al., 2012; Elliott et al., 2014; Rasmussen et al., 2014; Søgaard et al., 2015; Spivak et al., 2014). However, clinical trials of cure strategies are limited by our incomplete ability to measure changes in the viral reservoir, which is required to evaluate or predict the success of an intervention, and time to viral rebound remains the best indicator of intervention efficacy, despite the potential negative clinical impact of allowing the virus to rebound and spread (El-Sadr et al., 2006). Thus, virologic or immunologic factors, preferably antigen specific, associated with delayed viral rebound or viral remission could revolutionize our ability to develop more effective "cure" strategies.

While HDAC inhibitors induce modest HIV RNA expression *in vivo*, immunological profiling has noted weak associations with reservoir size and reactivation (Archin et al., 2012; Rasmussen et al., 2014; Søgaard et al., 2015). Analyses thus far have focused largely on changes in viral nucleic acid levels, reactivatable virus levels, and cellular immune activation (Olesen et al., 2015). However, accumulating evidence suggests that antibody function and glycosylation also vary with disease progression, marked by an enrichment of functional antibodies among individuals that spontaneously control HIV in the absence of antiretroviral therapy (ART; Ackerman et al., 2016; Fuchs et al., 2015). However, it is not known whether changes in antibody quality

and more desirably with antigen-specific antibody levels or function may also track with viral rebound.

Changes in antibody glycosylation have been linked to altered inflammation across diseases, in which changes in galactosylation of bulk (non-antigen specific) antibodies can predict rheumatic flares, contribute to innate immune activation (Axford et al., 1992; Rook et al., 1991), track with cancer prognosis (Theodoratou et al., 2016), shift with inflammation (Anthony and Ravetch, 2010), and even track with aging (Krištić et al., 2014). Changes in galactosylation have been noted in HIV infection on bulk antibodies (Ackerman et al., 2013; Moore et al., 2005), amplified on antigen-specific antibodies tracking with altered antibody effector function (Ackerman et al., 2013); however, whether changes in antibody function and/or glycosylation track with viral rebound following the discontinuation of therapy was unclear.

Thus, here, we comprehensively profiled both the functional and biophysical characteristics of HIV gp120 envelope (Env)-specific antibodies (Chung et al., 2015) in a clinical trial using panobinostat (PNB) for 8 weeks as a latency-reversing agent (Rasmussen et al., 2014) (Figure 1A). Nine of the 15 patients underwent analytical treatment interruption (ATI), and time to viral rebound was examined. Systems serology profiling of the Env-specific antibodies pointed to a shift in antibody Fc-glycosylation profiles with time to viral rebound. Moreover, the same gp120-specific Fc-glycan profile was also associated with time to rebound in 2 additional separate HIV cohorts, pointing to the broader application of this HIV-specific antibody profile, across interventions, as a potential surrogate to potentially guide future HIV reservoir-directed interventions.

RESULTS

Dynamics of Antibody Effector Functions

During latency reversal, potent enough to cause increases in plasma virus, HIV envelope proteins may be transiently expressed on the surface of infected cells (Bruel et al., 2016; Wu et al., 2017), rendering virus-expressing cells vulnerable to detection by antibodies able to interact and drive innate immune activation or effector functions. Thus, to begin to explore whether a unique functional antibody profile may track selectively with differential viral rebound time, the ability of HIV gp120 Env-specific immunoglobulin G (IgG) to drive antibody-dependent natural killer (NK) cell activation (CD107a, interferon-γ [IFN-γ], and macrophage inflammatory protein-1β [MIP-1β] expression), NK cell-mediated antibody-dependent cellular cytotoxicity (ADCC), AD cellular phagocytosis (ADCP), AD complement deposition (ADCD), and AD neutrophil phagocytosis (ADNP) were interrogated over the PNB study period.

Modest but significant increases in ADCD (v6: 1.5-fold, $p = 0.026$; v12: 1.7-fold, $p = 0.026$; median) as well as ADCP (v6: 1.2-fold, $p = 0.009$; median) were observed during PNB treatment compared to baseline (v1) (Figure 1B); however, no change in overall function was observed across the cohort over the course of treatment. Conversely, individual changes were observed, when functional changes were interrogated over the study period, highlighting interindividual variation in response to treatment, especially seen for ADNP and ADCD (Figure 1B). However, we cannot rule out that these changes were due to natural variation in functional antibody profiles, as the study had no placebo group.

Given these inter-individual differences across functions, we next assessed the relationship of each effector function with time to viral rebound. Distinct relationships were observed across the functions, where some functions trended toward correlations with prolonged viral suppression, and others, including ADCP, pointed toward more rapid rebound (Figure 1C). Importantly, these associations were often transiently amplified during the period of PNB administration. Similar trends were observed looking at changes in function across time points or using overall area under the curve (AUC) to capture study period changes in antibody function over the PNB treatment period.

To identify features that tracked most significantly with viral rebound kinetics, we applied an unbiased penalty-based multivariate approach (elastic net/partial least squares regression [PLSR] model) (Zou and Hastie, 2005), aiming to identify a minimal set of antibody functions associated with time to rebound. The model identified 6 functional features, including ADNP (neutrophil) and ADCD (complement) antibody activity, as the 2 features that were most critical for separating individuals with slow rebound from individuals that rebounded rapidly (Figures 1D, 1E, and S1A–S1D).

These data suggest that changes in HIV Env-specific ADCD and ADNP during the PNB treatment period were linked with a longer time to viral rebound, unrelated to CD4 counts, CD4 nadir, or transient virema (Figure S1E). However, as a single time point measurement, the functional activity at the time of ART interruption (v12) was not an accurate predictor of time to viral rebound ($R^2 = 0.28$, with cross-validation) (Figure S1C).

Antibody Glycosylation Tracks with Viral Rebound

To further define whether specific biophysical humoral changes contributed to the observed functional associations, we next sought to characterize the Fc-linked biophysical changes in HIV-specific antibodies across subjects that tracked with rebound kinetics.

HIV-specific IgG titers were stable over the course of the study period across all of the subjects (Figures S2A and S2B) and correlated with some effector functions. Conversely, titers did not associate with ADNP and ADCD (Figure S2C), suggesting that qualitative, rather than quantitative, changes in the Env-specific response must account for differential ADNP and ADCD activity.

Two modifications were made to the Fc-domain tune antibody effector activity: (1) changes in antibody isotype/subclass levels and (2) changes in antibody Fc N-glycosylation (Arnold et al., 2007). While we observed no differences in IgG subclass distribution over the study period (Figures S2B and S2D), the Fc N-linked glycans on Env-specific IgG conversely showed variation following PNB treatment. Compared to baseline (v1), we observed minor decreases in agalactosylated (G0) IgG (v6: 0.94-fold, $p = 0.0024$; v9: 0.88-fold, $p = 0.004$; v12: 0.92-fold, $p = 0.024$). In contrast, increases were observed in di-galactosylated (G2) (v9: 1.05-fold; $p = 0.013$; v12: 1.06-fold, $p = 0.048$; median), as well as fucosylated IgG glycans (v12: 1.03, $p = 0.007$) (Figure 2A).

CellPress
OPEN ACCESS

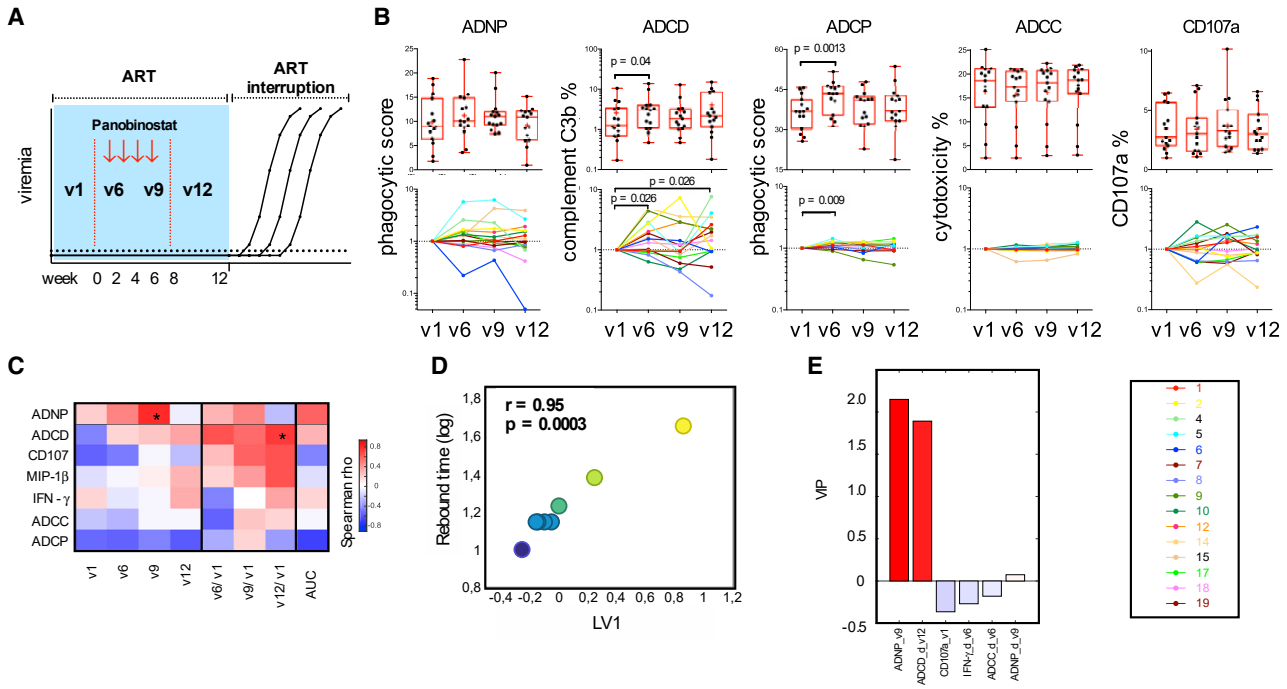

Figure 1. Extra-neutralizing Effector Functions Induced by HIV gp120-Specific IgG Are Associated with Viral Rebound during PNB Treatment

HIV gp120-specific antibodies were isolated from plasma samples and assessed for functional activity.

(A) Schematic study overview. Shaded area indicates antiretroviral treatment (ART) before analytical treatment interruption. The panobinostat (PNB) treatment period is indicated by red arrows. Sample time points are indicated as baseline (v1), on PNB treatment (v6 and v9), follow-up, and last time point before ATI (v12). "Rebound time" is defined as the time from ART interruption to detectable viremia.

(B) Upper panel: whisker boxplots depict HIV gp120 antibody-directed effector functional profiles over the study period (Wilcoxon test; only significant p values related to v1 are shown; n = 15; boxes: median, 25th and 75th percentile; whiskers: range). Lower panel: line plots depict relative change in HIV gp120 antibody-directed effector functional profiles over the study period (Wilcoxon signed rank test; only changes related to v1 were tested; n = 15); ACDC, antibody-dependent complement deposition; ADCC, AD cellular cytotoxicity; ADCP, AD cellular phagocytosis (monocytic); ADNP, antibody-dependent neutrophil phagocytosis. CD107a: AD NK cell degranulation. MIP-1β and IFN-γ: intracellular NK cell staining.

(C) Heatmap depicts association of antibody-induced effector functions and rebound time throughout the study at individual time points, changes from baseline, and area under the curve (AUC) for the entire study period for the patients who underwent treatment interruption (Spearman; * = false discovery rate [FDR]-adjusted $p < 0.05$; n = 9).

(D and E) To apply an unbiased identification of the most important functional features, elastic net identified 6 features that were most associated with time to viral rebound during the entire study (PLSRcoefficient $R^2 = 0.98$; leave-1-out cross-validation; n = 9).

(D) LV1 scores from the PLSR model versus rebound time (Spearman).

(E) Variable importance plot (VIP) depicts the importance of the selected features in the PLSR model in relation to rebound time. Red color indicates a positive coefficient, while blue color indicates a negative coefficient.

See also Figure S1.

Importantly, Env-specific G2 glycan levels at the time of treatment discontinuation (v12) were significantly associated with increased time to viral rebound (r = 0.94; p = 0.008). Furthermore, Env-specific sialylated IgG was also associated with a longer time to rebound (r = 0.77; p = 0.018), while agalactosylated (G0) IgG levels were inversely correlated with time to rebound (r = −0.71; p = 0.036) (Figure 2B). Thus, these data argue for a significant relationship between Env-specific glycosylation profiles and time to viral rebound after discontinuation of ART.

Four mono-saccharides (galactose [G], fucose [F], sialic acid [S], and bisecting n-acetylglucosamine [B]) can be added in different combinations post-translationally to the antibody Fc-glycan, theoretically giving rise to up to 36 distinct glycan structures that may be attached to the Fc domain of an antibody (Arnold et al., 2007). Thus, using a penalty-based elastic net/PLSR model, able to account for collinearity, we next focused on the time point just prior to treatment discontinuation (v12), to define whether specific glycan profiles could be associated with viral rebound.

Seven glycan features were selected by the elastic net/PLSR model. Together, these glycans strongly linked with time to viral rebound (R^2 = 0.81; with cross-validation)(R^2 = PLSR coefficient). The di-galactose (G2) levels, monosialylated (S1) and non-bisecting variants of the G2 glycan all associated with longer time to rebound. Conversely, bisecting, G0 and G1 glycan structures were associated with more rapid rebound (Figures 2C and S2E–S2G). Moreover, to further investigate the potential association of these glycans with functional profiles, a network analysis highlighted the core linked relationship between G2 glycans and ADCD/ADNP activity (Figure 2D) (the only 2 functions linked to

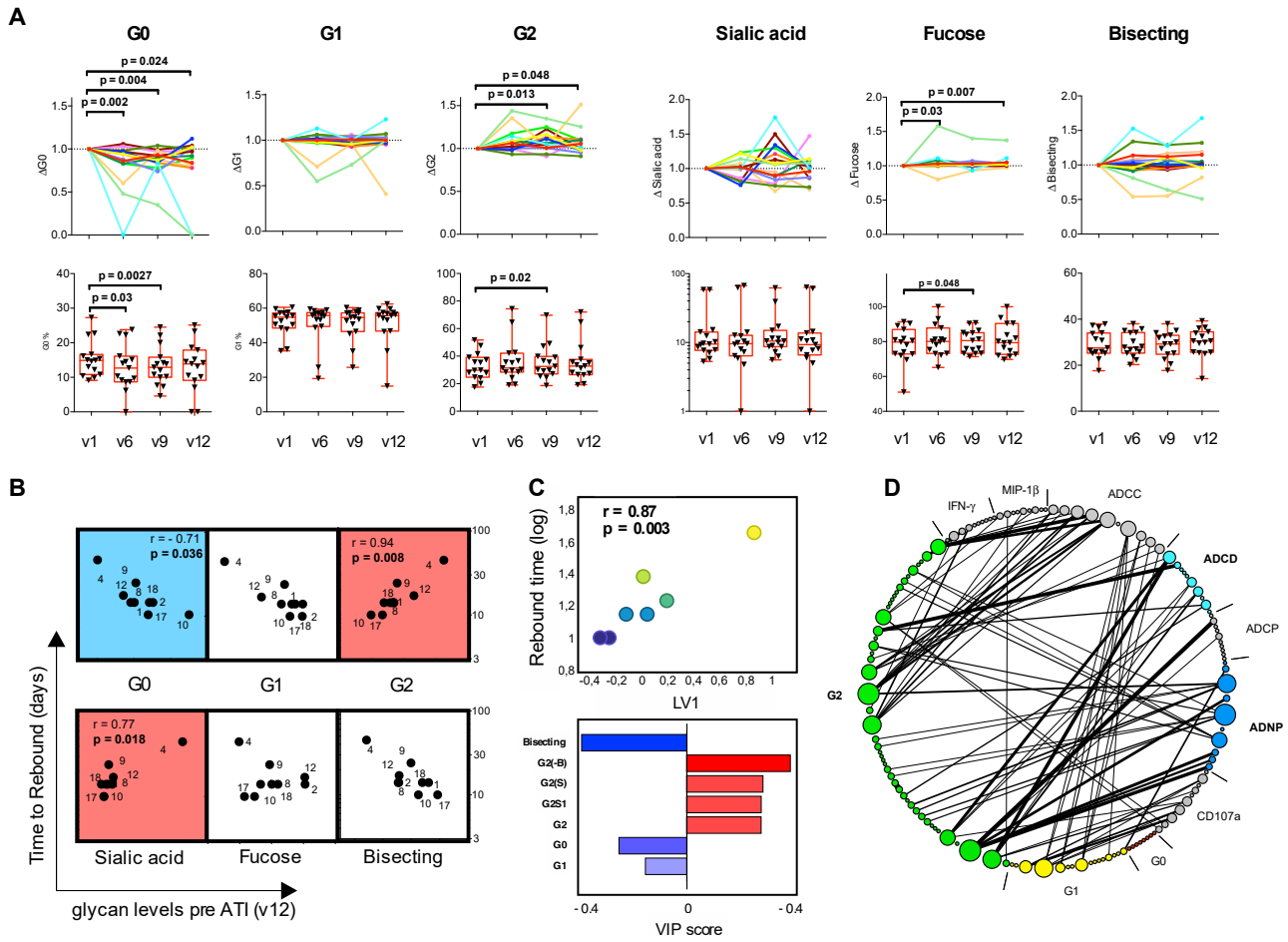

Figure 2. Glycosylation of HIV-1 gp120-Specific IgG Tracks with Viral Rebound Time after Treatment Interruption

HIV-1 gp120-specific IgG was isolated from plasma samples and Fc-n-linked glycans were profiled by capillary electrophoresis.

(A) Upper panel: line plots depict relative change in major glycan groups on HIV gp120-specific antibodies from baseline (v1) throughout the study across all of the subjects. Non-galactosylated (G0), monogalactosylated (G1), and digalatosylated (G2), as well as sialylated, fucosylated, and bisecting glycans (Wilcoxon signed rank test; only changes related to v1 were tested; n = 15); lower panel: the boxplots depict the raw data of the major glycan groups, non-galactosylated (G0), monogalactosylated (G1), and digalatosylated (G2) throughout the study across all of the subjects, as well as sialylated, fucosylated, and bisecting glycans (Wilcoxon test; only significant p values related to v1 are shown; n = 15; boxes: median, 25th and 75th percentile; whiskers: range).

(B) The correlation plots depict the relationships between the antibody glycan profile before treatment interruption (v12) and time to viral rebound (Spearman correlation; each dot is labeled with patient identification number; n = 9).

(C) Of all of the major and minor glycan groups at v12 (pre-ATI time point), elastic net identified 7 features that together had the strongest linkage with time to viral rebound (PLSR coefficient R^2 = 0.81; leave-1-out cross-validation; n = 9). (Upper panel) LV1 scores from the PLSR model versus rebound time (Spearman r). (Lower panel) Variable importance plot (VIP) depicts the importance of the selected features in the PLSR model in relation to rebound time. Red indicates a positive coefficient, while blue indicates a negative coefficient.

(D) Network analysis, which comprehensively interrogated the correlation of any pair of the glycan and the function across the study time points, consistently highlighted the direct core relationship between G2 and ADCD/ADNP functions. Edges are weighted by the correlation coefficient. Node size is determined by weight. For better visualization, only positive correlations are shown, and intra-correlations within glycans and functions are removed.

viral rebound time; see also Figure 1E), confirming the intimate relationship between functional and glycan changes that track with viral rebound. Finally, an overall elastic net-PLSR model built on all captured HIV-specific antibody changes confirmed these associations with rebound time (R^2 = 0.99; $p < 0.001$) (Figures S2H–S2J).

Validation in Independent HIV Cohorts

Due to ethical considerations (Julg et al., 2019), reactivation studies are small in size. Thus, to interrogate the robustness of the Env-specific glycan profile that associated with rebound times following PNB treatment, we elected to test the robustness of the glycan correlate in the most stringent manner possible, via orthogonal blinded validation in a separate population. Thus, we next tested whether the same changes also tracked with rebound kinetics in a second, independent cohort of early-treated HIV patients, in which individuals underwent cycles of analytic supervised treatment interruptions (STIs), hypothesized to drive auto-immunization and spontaneous viral control (Kaufmann et al., 2004; Rosenberg et al., 2000) (Figure S3A). Four of

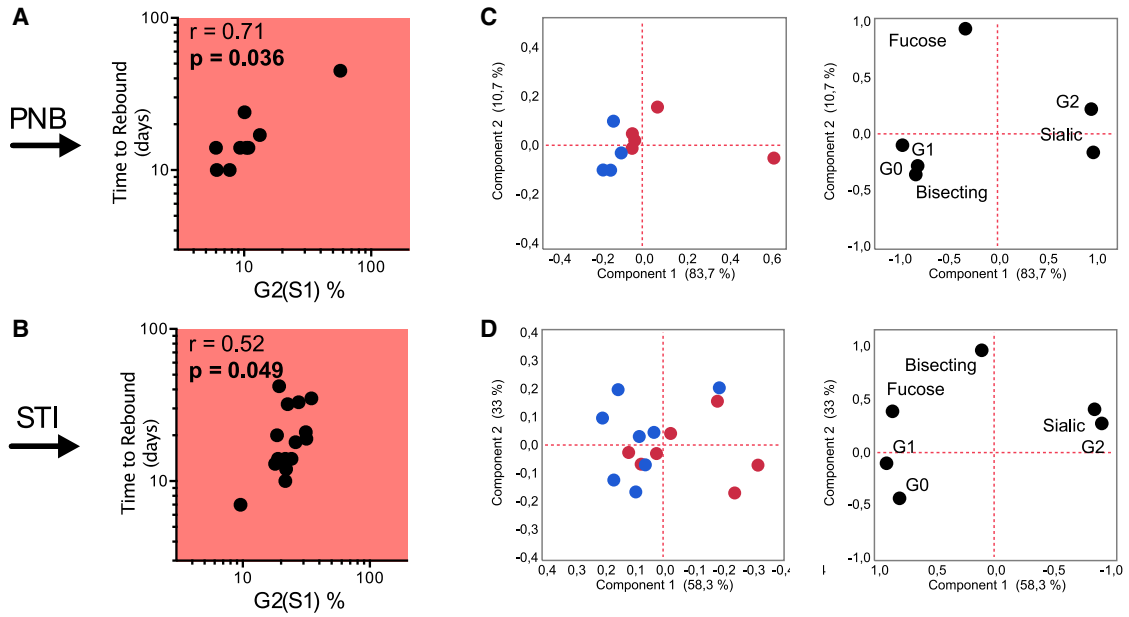

Figure 3. Validation of HIV-1 gp120-Specific IgG Glycosylation Patterns across Independent HIV Cohorts

(A and B) Spearman correlation of G2(S1) and rebound time for the PNB (pre-ATI, v12) and the STI HIV cohort.

(C and D) PCA analysis on major glycan groups. Together, PC1 and PC2 captured 94% of the variation for the PNB cohort (C) (pre-ATI, v12), and 91% for STI cohort (D). Blue dots indicate short rebound, while red dots indicate long rebound groups. (PNB: n = 9; STI: n = 15).

the patients were sampled after ATI, and 3 patients had already rebounded.

The same G2(S1) glycan, identified in the PNB cohort, was significantly correlated with rebound time in both cohorts (PNB v12: r = 0.71, p = 0.036; STI: r = 0.52, p = 0.049) (Figures 3A and 3B). Furthermore, the overall level of the major glycan groups could in fact separate individuals with rapid versus slower rebound in an unsupervised principal-component analysis (PCA), with PC1 and PC2 together capturing 94% of the variance in viral rebound time in the PNB cohort and 91% in the STI cohort (Figures 3C and 3D). Importantly, while even subtle glycan changes are known to drive differences in functional activity (Nimmerjahn et al., 2007; Peipp et al., 2008), the overall antibody-glycan profile did not change dramatically over the course of PNB treatment, highlighting the specificity of the glycan changes, occurring only within the HIV-specific antibody compartment (Figure S3B) (Rasmussen et al., 2014).

To even further validate this glycan profile and determine whether the same biomarkers could also be used to track rebound times in individuals that had already interrupted ART, we next sought to define whether the same HIV-specific glycan profile tracked with rebound in a third independent HIV cohort. The patients participated in a therapeutic HIV vaccine study to evaluate the safety and immunogenicity of an HIV-1 DNA vaccine (VRC-HVDNA 009-00-VP) aimed at driving therapeutic control of viremia in subjects treated with ART during acute/early HIV-1 infection (Rosenberg et al., 2010) (Figure S3C). Specifically, plasma samples from 9 patients were profiled 4 weeks post-ATI, all of them before viral rebound had occurred. While this sampling time point was distinct from those collected in the PNB and STI cohort, with a higher probability of exposure to early rebounding virus, the same G2(S1) signature was enriched among individuals that rebounded more slowly (r = 0.86, p = 0.004) (Figure 4A). Even combining the G2(S1) from all 3 independent cohorts into a single meta-like-analysis, the correlation with rebound time remained highly significant (r = 0.54, p = 0.001) (Figure S3D), further illustrating that the initially suspected "outliers" from the first 2 cohorts were in fact less likely to be actual outliers, but instead, the actual behavior of unique subjects able to control their reservoir for prolonged periods of time.

Finally, a model built on the major glycan groups could also separate individuals with rapid versus slower rebound in a PCA (Figure 4B), in which PC1 and PC2 together were able to capture 89% of the total variation. These data highlight the broad applicability of this glycan profile across 3 distinct interventions as well as before or after discontinuation of therapy.

Plasmablasts Links HIV Transcriptional Activity and G2 Glycans

Finally, to explore the biological basis for the link between the G2 signature and viral rebound, we next sought to define the relationships between immunophenotypic B cell profiles, HIV-specific antibody glycosylation, viral transcription, and rebound time from the reactivated latent reservoir. Network analyses revealed linkages between plasmablasts, unspliced HIV RNA levels, and glycosylation changes (Figure 5A), pointing to a pool of plasmablasts potentially harboring stable glycan profiles until viral reactivation occurs, marked by increased viral RNA transcript levels. Univariate analyses further confirmed the significant relationship between early viral transcript levels at the time of treatment discontinuation, plasmablast frequencies, and G2 levels (Figures 5B–5D).

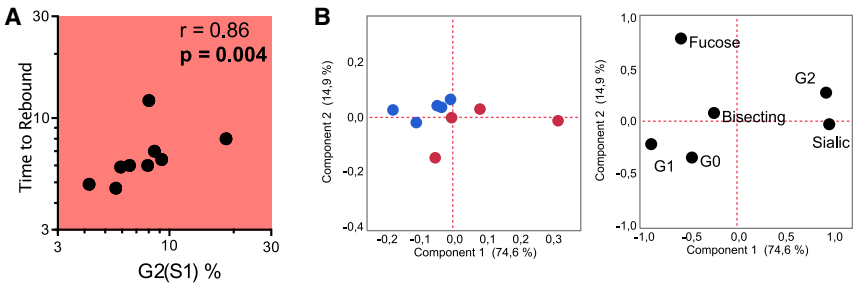

Figure 4. Fc-N-Linked Glycans on HIV gp120-Specific IgG Confirms Same Pattern in a Vaccine HIV Cohort Undergoing ATI

(A) Spearman rank correlation of G2(S1) glycan levels and rebound time for the ATI cohort.

(B) PCA analysis on major glycan groups. Together, PC1 and PC2 captured 89% of the variation for the ATI cohort (n = 9).

To further explore the relationship between antibody galactosylation and plasmablast levels, we analyzed the expression of glycosylation gene profiles in B cells from HIV$^-$ patients following influenza vaccination at day 0 and again at day 7, when plasmablasts peak. As expected, galactose transferase expression was significantly elevated at day 7, when plasmablasts are highly expanded (Figure S3E), suggestive of specific changes in galactosylation as plasmablasts form in response to antigen exposure. These data point to the potential role of patrolling memory B cells acting as early biosensors of early viral reactivation deep within tissues, where they may sense minute amounts of antigen and rapidly convert phenotype to antibody-secreting cells able to generate antibodies with a unique glycan signature. Given that plasmablasts are able to generate thousands of antibodies per second (Helmreich et al., 1961; Hibi and Dosch, 1986), the selective conversion of Env-specific B cells among subjects with some viral reactivation could rapidly repopulate the peripheral circulation with altered HIV-specific glycosylated antibodies, acting as a marker of B cell conversion and antiviral immunity.

DISCUSSION

Despite the intense interest in the development of shock and kill strategies aimed at activating and then killing the latent reservoir, a deep understanding of the interplay between latent virus, reactivation, and immune responses are still lacking. While several virologic assays have been developed to specifically probe the level of "reactivatable" virus in latently infected cells on ART (REFs), these assays continue to track poorly with time to rebound. Here, we show that a simple HIV-specific antibody post-translational glycan shift, linked to alterations in antibody effector function, tracks with rebound kinetics across 3 independent ART discontinuation studies.

Specifically, HIV Env-specific sialylated G2 glycans were found to be associated with viral rebound across 3 different interventional studies, suggesting that these antibody profiles are independent of the latency reversal approach used. Instead, the glycan profile may simply reflect a generic response from the humoral immune response upon early detection of reservoir activity. Given that changes in glycan profiles were linked to altered plasmablast frequencies, these data suggest that altered HIV-specific antibody glycosylation may be a reflection of a unique glycan profile that emerges following early B cell activation from plasmablasts. Because memory B cells can circulate and probe tissues throughout the body, the association between plasmablast frequencies, G2 levels, and early viral transcripts point to the possible activation of memory B cells by reservoir activity deep within tissues that may be unavailable to traditional reservoir-monitoring strategies. Moreover, digalactosylated and sialylated antibody glycans have been linked to plasmablasts following vaccination (Selman et al., 2012; Wang et al., 2015), pointing to the highly specialized nature of this glycan as a marker of B cell activation and maturation into an antibody-secreting cell. Because plasmablasts are able to secrete thousands of antibodies per second (Helmreich et al., 1961; Hibi and Dosch, 1986), differentiation of these may not alter the overall level of antibody in the context of hypergammaglobulinemia (De Milito et al., 2004), but may provide a simple change in peripheral antigen-specific antibody glycan profiles, due to the highly specialized antibody glycans they produce. Thus, our findings point to a potentially informative role for changes in HIV-specific antibody post-translational modifications in glycosylation as a novel indicator of early B cell activation in response to reservoir activity, even deep within a viral sanctuary.

While the available cohorts studied here are small in number, we took several approaches to ensure orthogonal statistical validation of our findings in the most stringent ways possible. First, we applied several methods to validate our findings by using basic univariate non-parametric tests and confirmed these findings with independent and more complex supervised as well as unsupervised multivariate models—all consistently confirming that the same patterns were associated with time to rebound, offering the most stringent internal validation. Second, the associations observed were replicated across 3 completely independent HIV treatment interruption studies, confirming the similar antibody signatures in all of the cohorts associated with time to rebound and emphasizing that the signature is not altered by cohort variation. Finally, we included cohorts of individuals pre- and post-rebound, in which levels of viremia may differ, but continued to observe the same statistical significance, arguing that the analysis of this glycan change remains predictive before and aftertreatment discontinuation, highlighting the potential use, in conjunction with established reservoir models, to further understand HIV reservoir dynamics. Consistent with the emerging association of antibody glycosylation changes with reservoir size across a fourth independent cohort (Vadrevu et al., 2018), the data presented here point to the potential utility to track not only reservoir size but also reservoir reactivation. Thus, the quantification of HIV-specific glycan profiles offers a simple, easily accessible, and

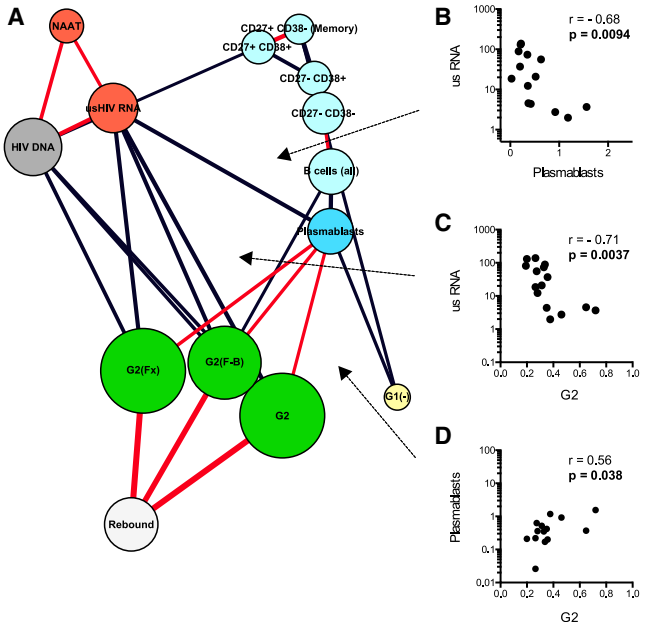

Figure 5. Plasmablasts Link HIV Transcriptional Activity and G2 Glycans

(A) Network analysis depicts connections among HIV reservoir size, its transcriptional activity, B cells/plasmablasts, and glycans. Nodes represent the features. The red edges indicate significant positive associations, while the black indicate inverse associations.

(B–D) Highlighted correlations are shown for plasmablasts versus unspliced HIV RNA, G2 glycans versus unspliced HIV RNA, and plasmablasts versus G2 glycans (Spearman correlation; n = 15).

inexpensive test to monitor reservoir activity in a sensitive and specific manner.

Whether gp120 Env-specific antibody glycoforms are simply markers of early reservoir activity or are also mechanistically involved in viral control, or even reservoir reduction, is not clear. While several lines of evidence suggest that antibody function may directly affect the reservoir (Lu et al., 2016), the changes noted here may merely be a reflection of changes in B cell differentiation in response to viral reactivation, rather than to antibody effector functions that may track with anti-reservoir activity. However, emerging data do point to lymphoid tissues—and specifically germinal centers (GCs), largely composed of B cells—as critical reservoirs for the virus (Fukazawa et al., 2015). While $CD8^+$ T cells and NK cells are rarely able to penetrate these vulnerable inductive sites (Connick et al., 2007), recent data suggest that complement (Zwirner et al., 1989) and neutrophils (Sips et al., 2016) are highly abundant within these sites, potentially reflecting unexpected antibody effector functions that could contribute to anti-reservoir activity upon the production of highly functional antibodies. Thus, future *in vivo* models and potential clinical studies may further elucidate whether these antibody properties are only simple markers or also mechanistic contributors to reservoir control.

Although NK cell-mediated ADCC was not predictive of viral rebound time, these results do not preclude the potentially critical contribution of NK cells in viral control and ultimate eradication. Along these lines, studies using an NK cell-killing ADCC assay likewise did not observe an association between ADCC and viral rebound time (Lee et al., 2017). However, a recent successful monoclonal antibody and latency reversing agent (LRA) approach pointed to NK cell and granulocyte activation as critical predictors of delayed rebound time in non-human primates (Borducchi et al., 2018). Thus, these data suggest that while ADNP and ADCD alone were linked to viral rebound time in our study, other antibody effector functions may also ultimately contribute to the eradication of the viral reservoir.

HIV-specific antibody glycosylation can be readily measured with high-throughput methods (Mahan et al., 2015) and these Fc-N-linked glycosylation profiles offer a novel means to understand, customize, and tailor eradication strategies. Other HIV-specific antibody subpopulations targeting distinct gp120 Env epitopes, early Tat, or abundant p24 may also serve as more sensitive immune signatures and warrant further investigation in larger cohorts. In conclusion, these findings provide the foundation for the future development of this promising tool to study latent viral pathogen-host interplay in HIV infection and potentially in other chronic viral infections and virus-induced cancers.

STAR★METHODS

Detailed methods are provided in the online version of this paper and include the following:

- KEY RESOURCES TABLE
- RESOURCE AVAILABILITY
  - Lead Contact
  - Materials Availability
  - Data and Code Availability
- EXPERIMENTAL MODEL AND SUBJECT DETAILS
  - Panobinostat cohort
  - STI HIV-cohort
  - HIV vaccine ATI cohort
  - Influenza vaccine cohort
- METHOD DETAILS
  - Antibody-Dependent Cellular Phagocytosis (ADCP)
  - Antibody-Dependent Neutrophil Phagocytosis (ADNP)
  - Antibody-dependent cellular cytotoxicity (ADCC) assay
  - Antibody-dependent complement deposition (ADCD)
  - Antibody-dependent NK cell activation
  - Luminex Isotype Assay
  - Glycan analysis of anti-HIV-specific IgG
  - B cell sorting
  - B cell flow cytometry, HIV DNA and usHIV RNA for the PNB cohort

- QUANTIFICATION AND STATISTICAL ANALYSIS
  - Construction of correlation network
  - Identification of the viral rebound specific correlates with Elastic-Net/PLSR
  - Additional statistical methods

SUPPLEMENTAL INFORMATION

Supplemental Information can be found online at https://doi.org/10.1016/j.celrep.2020.108502.

ACKNOWLEDGMENTS

We would like to thank the Ragon Institute of MGH, MIT and Harvard, the Harvard Center for AIDS Research, the Massachusetts General Hospital Research Scholar Program, and Dr. Daniel Wattendorf for their support.

AUTHOR CONTRIBUTIONS

G.A. devised the research idea, study design, and concept. R.O., M.F.J., C.L., and J.S. performed the glycan isolation and analysis. R.O., Z.E., G.L., and S.F. performed the functional assays. S.V. and M.L. performed the B cell phenotyping. S.S. and D.D.-G. performed the B cell phenotyping and sorting. L.Z. performed the statistical analysis. T.A.R., L.Ø., M.T., O.S.S., E.P.S., E.S.R., K.E.S., and D.H.B. contributed plasma samples. R.C.C. performed and collected flu vaccine studies and peripheral blood mononuclear cell (PBMC) collections. R.O., W.-H.Y., and G.A. analyzed and interpreted the data. R.O., B.J., and G.A. wrote the manuscript. All of the authors critically reviewed the manuscript. G.A. supervised all aspects of this study.

DECLARATION OF INTERESTS

G.A. has a financial interest (founder) in SeromYx, a company developing platform technology that describes the antibody immune response. G.A.'s interests were reviewed and are managed by Massachusetts General Hospital and Partners HealthCare in accordance with their conflict of interest policies. The other authors declare no competing interests.

Received: April 14, 2020
Revised: July 22, 2020
Accepted: November 18, 2020
Published: December 15, 2020

REFERENCES

Ackerman, M.E., Crispin, M., Yu, X., Baruah, K., Boesch, A.W., Harvey, D.J., Dugast, A.-S., Heizen, E.L., Ercan, A., Choi, I., et al. (2013). Natural variation in Fc glycosylation of HIV-specific antibodies impacts antiviral activity. J. Clin. Invest. *123*, 2183–2192.

Ackerman, M.E., Mikhailova, A., Brown, E.P., Dowell, K.G., Walker, B.D., Bailey-Kellogg, C., Suscovich, T.J., and Alter, G. (2016). Polyfunctional HIV-Specific Antibody Responses Are Associated with Spontaneous HIV Control. PLOS Pathog. *12*, e1005315.

Anthony, R.M., and Ravetch, J.V. (2010). A novel role for the IgG Fc glycan: the anti-inflammatory activity of sialylated IgG Fcs. J. Clin. Immunol. *30* (*Suppl 1*), S9–S14.

Archin, N.M., Liberty, A.L., Kashuba, A.D., Choudhary, S.K., Kuruc, J.D., Crooks, A.M., Parker, D.C., Anderson, E.M., Kearney, M.F., Strain, M.C., et al. (2012). Administration of vorinostat disrupts HIV-1 latency in patients on antiretroviral therapy. Nature *487*, 482–485.

Arnold, J.N., Wormald, M.R., Sim, R.B., Rudd, P.M., and Dwek, R.A. (2007). The impact of glycosylation on the biological function and structure of human immunoglobulins. Annu. Rev. Immunol. *25*, 21–50.

Axford, J.S., Sumar, N., Alavi, A., Isenberg, D.A., Young, A., Bodman, K.B., and Roitt, I.M. (1992). Changes in normal glycosylation mechanisms in autoimmune rheumatic disease. J. Clin. Invest. *89*, 1021–1031.

Borducchi, E.N., Liu, J., Nkolola, J.P., Cadena, A.M., Yu, W.-H., Fischinger, S., Broge, T., Abbink, P., Mercado, N.B., Chandrashekar, A., et al. (2018). Antibody and TLR7 agonist delay viral rebound in SHIV-infected monkeys. Nature *563*, 360–364.

Bruel, T., Guivel-Benhassine, F., Amraoui, S., Malbec, M., Richard, L., Bourdic, K., Donahue, D.A., Lorin, V., Casartelli, N., Noël, N., et al. (2016). Elimination of HIV-1-infected cells by broadly neutralizing antibodies. Nat. Commun. *7*, 10844.

Cawley, G.C., and Talbot, N.L.C. (2010). On Over-fitting in Model Selection and Subsequent Selection Bias in Performance Evaluation. J. Mach. Learn. Res. *11*, 2079–2107.

Chung, A.W., Ghebremichael, M., Robinson, H., Brown, E., Choi, I., Lane, S., Dugast, A.-S., Schoen, M.K., Rolland, M., Suscovich, T.J., et al. (2014). Polyfunctional Fc-effector profiles mediated by IgG subclass selection distinguish RV144 and VAX003 vaccines. Sci. Transl. Med. *6*, 228ra38.

Chung, A.W., Kumar, M.P., Arnold, K.B., Yu, W.H., Schoen, M.K., Dunphy, L.J., Suscovich, T.J., Frahm, N., Linde, C., Mahan, A.E., et al. (2015). Dissecting Polyclonal Vaccine-Induced Humoral Immunity against HIV Using Systems Serology. Cell *163*, 988–998.

Connick, E., Mattila, T., Folkvord, J.M., Schlichtemeier, R., Meditz, A.L., Ray, M.G., McCarter, M.D., Mawhinney, S., Hage, A., White, C., et al. (2007). CTL fail to accumulate at sites of HIV-1 replication in lymphoid tissue. J.I Immunol. *178*, 6975–6983.

De Milito, A., Nilsson, A., Titanji, K., Thorstensson, R., Reizenstein, E., Narita, M., Grutzmeier, S., Sönnerborg, A., and Chiodi, F. (2004). Mechanisms of hypergammaglobulinemia and impaired antigen-specific humoral immunity in HIV-1 infection. Blood *103*, 2180–2186.

El-Sadr, W.M., Lundgren, J., Neaton, J.D., Gordin, F., Abrams, D., Arduino, R.C., Babiker, A., Burman, W., Clumeck, N., Cohen, C.J., et al.; Strategies for Management of Antiretroviral Therapy (SMART) Study Group (2006). CD4+ count-guided interruption of antiretroviral treatment. N. Engl. J. Med. *355*, 2283–2296.

Elliott, J.H., Wightman, F., Solomon, A., Ghneim, K., Ahlers, J., Cameron, M.J., Smith, M.Z., Spelman, T., McMahon, J., Velayudham, P., et al. (2014). Activation of HIV transcription with short-course vorinostat in HIV-infected patients on suppressive antiretroviral therapy. PLOS Pathog. *10*, e1004473.

Finzi, D., Blankson, J., Siliciano, J.D., Margolick, J.B., Chadwick, K., Pierson, T., Smith, K., Lisziewicz, J., Lori, F., Flexner, C., et al. (1999). Latent infection of CD4+ T cells provides a mechanism for lifelong persistence of HIV-1, even in patients on effective combination therapy. Nat. Med. *5*, 512–517.

Fuchs, S.P., Martinez-Navio, J.M., Piatak, M., Jr., Lifson, J.D., Gao, G., and Desrosiers, R.C. (2015). AAV-Delivered Antibody Mediates Significant Protective Effects against SIVmac239 Challenge in the Absence of Neutralizing Activity. PLOS Pathog. *11*, e1005090.

Fukazawa, Y., Lum, R., Okoye, A.A., Park, H., Matsuda, K., Bae, J.Y., Hagen, S.I., Shoemaker, R., Deleage, C., Lucero, C., et al. (2015). B cell follicle sanctuary permits persistent productive simian immunodeficiency virus infection in elite controllers. Nat. Med. *21*, 132–139.

Galindo-Prieto, B., Eriksson, L., and Trygg, J. (2014). Variable influence on projection (VIP) for orthogonal projections to latent structures (OPLS). J. Chemometr. *28*, 623–632.

Gómez-Román, V.R., Florese, R.H., Patterson, L.J., Peng, B., Venzon, D., Aldrich, K., and Robert-Guroff, M. (2006). A simplified method for the rapid fluorometric assessment of antibody-dependent cell-mediated cytotoxicity. J. Immunol. Methods *308*, 53–67.

Helmreich, E., Kern, M., and Eisen, H.N. (1961). The secretion of antibody by isolated lymph node cells. J. Biol. Chem. *236*, 464–473.

Hibi, T., and Dosch, H.-M. (1986). Limiting dilution analysis of the B cell compartment in human bone marrow. Eur. J. Immunol. *16*, 139–145.

Julg, B., Dee, L., Ananworanich, J., Barouch, D.H., Bar, K., Caskey, M., Colby, D.J., Dawson, L., Dong, K.L., Dubé, K., et al. (2019). Recommendations for analytical antiretroviral treatment interruptions in HIV research trials-report of a consensus meeting. Lancet HIV *6*, e259–e268.

Kaufmann, D.E., Lichterfeld, M., Altfeld, M., Addo, M.M., Johnston, M.N., Lee, P.K., Wagner, B.S., Kalife, E.T., Strick, D., Rosenberg, E.S., and Walker, B.D. (2004). Limited durability of viral control following treated acute HIV infection. PLOS Med. *1*, e36.

Krištić, J., Vučković, F., Menni, C., Klarić, L., Keser, T., Beceheli, I., Pučić-Baković, M., Novokmet, M., Mangino, M., Thaqi, K., et al. (2014). Glycans are a novel biomarker of chronological and biological ages. J. Gerontol. A Biol. Sci. Med. Sci. *69*, 779–789.

Lee, W.S., Kristensen, A.B., Rasmussen, T.A., Tolstrup, M., Østergaard, L., Søgaard, O.S., Wines, B.D., Hogarth, P.M., Reynaldi, A., Davenport, M.P., et al. (2017). Anti-HIV-1 ADCC Antibodies following Latency Reversal and Treatment Interruption. J. Virol. *91*, e00603-17.

Li, B., and Dewey, C.N. (2011). RSEM: accurate transcript quantification from RNA-Seq data with or without a reference genome. BMC Bioinformatics *12*, 323.

Lu, C.L., Murakowski, D.K., Bournazos, S., Schoofs, T., Sarkar, D., Halper-Stromberg, A., Horwitz, J.A., Nogueira, L., Golijanin, J., Gazumyan, A., et al. (2016). Enhanced clearance of HIV-1-infected cells by broadly neutralizing antibodies against HIV-1 in vivo. Science *352*, 1001–1004.

Lun, A.T., Bach, K., and Marioni, J.C. (2016). Pooling across cells to normalize single-cell RNA sequencing data with many zero counts. Genome Biol. *17*, 75.

Mahan, A.E., Tedesco, J., Dionne, K., Baruah, K., Cheng, H.D., De Jager, P.L., Barouch, D.H., Suscovich, T., Ackerman, M., Crispin, M., and Alter, G. (2015). A method for high-throughput, sensitive analysis of IgG Fc and Fab glycosylation by capillary electrophoresis. J. Immunol. Methods *417*, 34–44.

Mahan, A.E., Jennewein, M.F., Suscovich, T., Dionne, K., Tedesco, J., Chung, A.W., Streeck, H., Pau, M., Schuitemaker, H., Francis, D., et al. (2016). Antigen-Specific Antibody Glycosylation Is Regulated via Vaccination. PLOS Pathog. *12*, e1005456.

McAndrew, E.G., Dugast, A.-S., Licht, A.F., Eusebio, J.R., Alter, G., and Ackerman, M.E. (2011). Determining the phagocytic activity of clinical antibody samples. J. Vis. Exp. (*57*), e3588.

Moore, J.S., Wu, X., Kulhavy, R., Tomana, M., Novak, J., Moldoveanu, Z., Brown, R., Goepfert, P.A., and Mestecky, J. (2005). Increased levels of galactose-deficient IgG in sera of HIV-1-infected individuals. AIDS *19*, 381–389.

Nimmerjahn, F., Anthony, R.M., and Ravetch, J.V. (2007). Agalactosylated IgG antibodies depend on cellular Fc receptors for in vivo activity. Proc. Natl. Acad. Sci. USA *104*, 8433–8437.

Olesen, R., Vigano, S., Rasmussen, T.A., Søgaard, O.S., Ouyang, Z., Buzon, M., Bashirova, A., Carrington, M., Palmer, S., Brinkmann, C.R., et al. (2015). Innate Immune Activity Correlates with CD4 T Cell-Associated HIV-1 DNA Decline during Latency-Reversing Treatment with Panobinostat. J. Virol. *89*, 10176–10189.

Peipp, M., Lammerts van Bueren, J.J., Schneider-Merck, T., Bleeker, W.W., Dechant, M., Beyer, T., Repp, R., van Berkel, P.H., Vink, T., van de Winkel, J.G., et al. (2008). Antibody fucosylation differentially impacts cytotoxicity mediated by NK and PMN effector cells. Blood *112*, 2390–2399.

Rasmussen, T.A., Tolstrup, M., Brinkmann, C.R., Olesen, R., Erikstrup, C., Solomon, A., Winckelmann, A., Palmer, S., Dinarello, C., Buzon, M., et al. (2014). Panobinostat, a histone deacetylase inhibitor, for latent-virus reactivation in HIV-infected patients on suppressive antiretroviral therapy: a phase 1/2, single group, clinical trial. Lancet HIV *1*, e13–e21.

Risso, D., Ngai, J., Speed, T.P., and Dudoit, S. (2014). Normalization of RNA-seq data using factor analysis of control genes or samples. Nat. Biotechnol. *32*, 896–902.

Rook, G.A., Steele, J., Brealey, R., Whyte, A., Isenberg, D., Sumar, N., Nelson, J.L., Bodman, K.B., Young, A., Roitt, I.M., et al. (1991). Changes in IgG glycoform levels are associated with remission of arthritis during pregnancy. J. Autoimmun. *4*, 779–794.

Rosenberg, E.S., Altfeld, M., Poon, S.H., Phillips, M.N., Wilkes, B.M., Eldridge, R.L., Robbins, G.K., D'Aquila, R.T., Goulder, P.J., and Walker, B.D. (2000). Immune control of HIV-1 after early treatment of acute infection. Nature *407*, 523–526.

Rosenberg, E.S., Graham, B.S., Chan, E.S., Bosch, R.J., Stocker, V., Maenza, J., Markowitz, M., Little, S., Sax, P.E., Collier, A.C., et al.; AIDS Clinical Trials Group A5187 Team (2010). Safety and immunogenicity of therapeutic DNA vaccination in individuals treated with antiretroviral therapy during acute/early HIV-1 infection. PLOS ONE *5*, e10555.

Selman, M.H.J., de Jong, S.E., Soonawala, D., Kroon, F.P., Adegnika, A.A., Deelder, A.M., Hokke, C.H., Yazdanbakhsh, M., and Wuhrer, M. (2012). Changes in Antigen-specific IgG1 Fc N-glycosylation Upon Influenza and Tetanus Vaccination. Mol. Cell. Proteomics *11*, M111, 014563.

Sips, M., Krykbaeva, M., Diefenbach, T.J., Ghebremichael, M., Bowman, B.A., Dugast, A.S., Boesch, A.W., Streeck, H., Kwon, D.S., Ackerman, M.E., et al. (2016). Fc receptor-mediated phagocytosis in tissues as a potent mechanism for preventive and therapeutic HIV vaccine strategies. Mucosal Immunol. *9*, 1584–1595.

Søgaard, O.S., Graversen, M.E., Leth, S., Olesen, R., Brinkmann, C.R., Nissen, S.K., Kjaer, A.S., Schleimann, M.H., Denton, P.W., Hey-Cunningham, W.J., et al. (2015). The Depsipeptide Romidepsin Reverses HIV-1 Latency In Vivo. PLOS Pathog. *11*, e1005142.

Spivak, A.M., Andrade, A., Eisele, E., Hoh, R., Bacchetti, P., Bumpus, N.N., Emad, F., Buckheit, R., 3rd, McCance-Katz, E.F., Lai, J., et al. (2014). A pilot study assessing the safety and latency-reversing activity of disulfiram in HIV-1-infected adults on antiretroviral therapy. Clin. Infect. Dis. *58*, 883–890.

Theodoratou, E., Thaçi, K., Agakov, F., Timofeeva, M.N., Štambuk, J., Pučić-Baković, M., Vučković, F., Orchard, P., Agakova, A., Din, F.V.N., et al. (2016). Glycosylation of plasma IgG in colorectal cancer prognosis. Sci. Rep. *6*, 28098.

Vadrevu, S.K., Trbojevic-Akmacic, I., Kossenkov, A.V., Colomb, F., Giron, L.B., Anzurez, A., Lynn, K., Mounzer, K., Landay, A.L., Kaplan, R.C., et al. (2018). Frontline science: plasma and immunoglobulin G galactosylation associate with HIV persistence during antiretroviral therapy. J. Leukoc. Biol. *104*, 461–471.

Verbyla, D.L., and Litvaitis, J.A. (1989). Resampling Methods for Evaluating Classification Accuracy of Wildlife Habitat Models. Environ. Manage. *13*, 783–787.

Wang, T.T., Maamary, J., Tan, G.S., Bournazos, S., Davis, C.W., Krammer, F., Schlesinger, S.J., Palese, P., Ahmed, R., and Ravetch, J.V. (2015). Anti-HA Glycoforms Drive B Cell Affinity Selection and Determine Influenza Vaccine Efficacy. Cell *162*, 160–169.

Wu, G., Swanson, M., Talla, A., Graham, D., Strizki, J., Gorman, D., Barnard, R.J.O., Blair, W., Søgaard, O.S., Tolstrup, M., et al. (2017). HDAC inhibition induces HIV-1 protein and enables immune-based clearance following latency reversal. JCI Insight *2*, 1–11.

Zou, H., and Hastie, T. (2005). Regularization and variable selection via the elastic-net. J. R. Stat. Soc. Ser. A Stat. Soc. *67*, 301–320.

Zwirner, J., Felber, E., Schmidt, P., Riethmüller, G., and Feucht, H.E. (1989). Complement activation in human lymphoid germinal centres. Immunology *66*, 270–277.

STAR★METHODS

KEY RESOURCES TABLE

REAGENT or RESOURCE	SOURCE	IDENTIFIER
Antibodies		
Anti-CD3 Alexa Fluor® 700 Mouse Anti-Human	BD	Cat#557943
Anti-CD14 APC-Cy7 Mouse Anti-Human; clone MφP9	BD	Cat#557831
Anti-CD16 APC-Cy7 Mouse Anti-Human; clone 3G8	BD	Cat#557758
Anti-CD56 PE-Cy7 Mouse Anti-Human	BD	Cat#557747
Anti-CD66b Pacific Blue Anti-Human; clone G10F5	Biolegend	Cat#305112
RosetteSep Human NK Cell Enrichment Cocktail	Stem Cell Technologies	Cat#15065
Anti-CD107a PE-Cy5	BD	Cat#555802
Anti-IFN-γ APC Mouse Anti-Human; Clone B27 (RUO)	BD	Cat#554702
Anti-MIP-1β, PE mouse Mouse Anti-	BD	Cat#550078
Anti-IgG PE	Southern Biotech	Cat#9040-09
Anti-IgG1 PE	Southern Biotech	Cat#9052-09
Anti-IgG2 PE	Southern Biotech	Cat#9070-09
Anti-IgG3 PE	Southern Biotech	Cat#9210-09
Anti-IgG4 PE	Southern Biotech	Cat#9200-09
Chemicals, Peptides, and Recombinant Proteins		
HIV gp120 (sf162)	Immune Technology	Cat#IT-001-0028p
Red Fluorescent Cell Linker	Sigma-Aldrich	Cat# PKH26GL-1KT
Brefeldin A	Sigma-Aldrich	Cat# B5936
GolgiStop	BD	Cat#554724
Peptide-N-Glycosidase F	New England Biolabs	Cat# P0704
8-aminopyrene-1,3,6-trisulfonic acid, trisodium salt	Invitrogen	Cat#A-6257
Glycanassure APTS	ThermoFischer	Cat#A28676
IdeZ Protease	New England Biolabs	Cat#p0770
Mag-SA beads	New England Biolabs	Cat#S1420S
Deposited Data		
Code generated during this study	This study	https://github.com/wenhan-yu/HIV_antibody_glycan
Experimental Models: Cell Lines		
THP-1 cells	ATCC	Cat#TIB-202
CEM.NKR CCR5+ Cells	NIH Aids Reagent Program	Cat#4376
Software and Algorithms		
MATLAB	Mathworks	RRID:SCR_001622
Prism software, version 6.0 for Mac	GraphPad	RRID:SCR_002798
JMP Pro v. 14.0.0	SAS Institute	N/A
Microsoft Excel for Mac v. 16.39	Microsoft	RRID:SCR_016137
xPONENT acquisition software	Bio-Rad	N/A
Gephi 0.9.2	Gephi	RRID:SCR_004293
FACSDiva software	BD	RRID:SCR_001456

(*Continued on next page*)

Continued

REAGENT or RESOURCE	SOURCE	IDENTIFIER
Bioplex Manager Software	Bio-Rad	RRID:SCR_014330
FlowJo 10.4 for Mac OS X	FlowJo, LLC	RRID:SCR_008520)
Other		
BD LSR II flow cytometer	BD	RRID:SCR_002159
Bio-Plex® 3D Suspension Array System	Bio-Rad	N/A
Applied Biosystems® Genetic Analyzer 3500 series	Applied Biosystems	N/A

RESOURCE AVAILABILITY

Lead Contact

Further information and requests for resources and reagents should be directed to and will be fulfilled by lead contact, Galit Alter (galter@mgh.harvard.edu).

Materials Availability

This study did not generate new unique reagents.

Data and Code Availability

The code generated during this study are available at https://github.com/wenhan-yu/HIV_antibody_glycan.

EXPERIMENTAL MODEL AND SUBJECT DETAILS

Panobinostat cohort

15 ART treated HIV-infected adults were enrolled (Rasmussen et al., 2014). Age: median (range): 47 (28-53). Sex: Male (100%). Race/ethnicity: white non-Hispanic: 15 (100%). Ethics committee approval was obtained in accordance with the principles of the Declaration of Helsinki. Each patient provided written informed consent. Patients received oral panobinostat (20 mg) three times per week every other week for 8 weeks. 9 of the 15 patients underwent ATI (clinicalTrials.gov, identifier: NCT01680094).

STI HIV-cohort

Samples from a single analytic supervised treatment interruption (STI) for 11 subjects and samples from two distinct STIs for two additional subjects, previously described (Kaufmann et al., 2004; Rosenberg et al., 2000), were included. Age: median (range): 36 (29-62) years. Sex: Male (100%). Race/ethnicity: Hispanic: 1 (8%), white non-Hispanic: 12 (92%). We selected samples encompassing the time period around the ATI. The median values for these samples relative to the start of the ATI were 0 days (range −26 to +21 days). The median rebound time for these samples was 18 days (range 7-42 days). All individuals gave written informed consent to participate, and the study was approved by the institutional review boards and conducted in accordance with the human experimentation guidelines of the Massachusetts General Hospital.

HIV vaccine ATI cohort

Samples from a clinical trial evaluating the safety and immunogenicity of an HIV-1 DNA vaccine (VRC-HVDNA 009-00- VP) in 9 subjects treated with ART during acute/early HIV-1 infection (clinicaltrials.gov identifier: NCT00125099), previously described (Rosenberg et al., 2010). Age: median (range): 40 (34-45) years. Sex: Male: 9 (100%). Race/ethnicity: White non-Hispanic: 7 (78%), Hispanic: 2 (22%). All subjects gave written informed consent, and the study protocol was approved by the AIDS Clinical Trials Group, the NIH Division of AIDS (DAIDS) and the human protection committees of each participating institution. Plasma samples were available from a time point four weeks post ATI.

Influenza vaccine cohort

PBMCs were collected at baseline and 7 days following routine influenza vaccination for 5 subjects. Age: median (range): 29 (25 - 60). Sex: Male: 3 (60%). All subjects gave written informed consent, and the study protocol was approved by the Massachusetts General Hospital.

METHOD DETAILS

Antibody-Dependent Cellular Phagocytosis (ADCP)

The cellular phagocytosis assay was performed as previously described (McAndrew et al., 2011). Biotinylated recombinant HIV gp120 (sf162) (Immune Technology) was coupled to 1 μm fluorescent neutravidin beads (Invitrogen) overnight at 4°C. Beads were

washed three times prior to incubation with purified IgG from individual donors in duplicate for 2 hr at 37°C. Next, monocytic THP-1 cells (ATCC) were added, and co-cultures were incubated overnight. Cells were washed and fixed in 4% PFA. Phagocytosis was measured by flow cytometry on a BD LSR II flow cytometer (for gating strategy see Figure S4) and a phagocytic score was calculated (frequency of bead-positive cells x MFI of bead fluorescence in same cells / 10^{-4}). Each sample was tested in two individual experiments.

Antibody-Dependent Neutrophil Phagocytosis (ADNP)

Neutrophils were isolated from whole blood from HIV-negative donor blood using dextran for 25 minutes. Supernatant was collected and remaining RBCs were lysed with dH_20 for 25 s, followed by rapid isotonic equilibration. Biotinylated recombinant HIV gp120 (sf162) (Immune Technology) was coupled to 1 μm fluorescent neutravidin beads (Invitrogen) overnight at 4°C. Beads were washed three times before incubated with purified IgG from individual donors in duplicate for 2 hr at 37°C. Neutrophils were then added and incubated with opsonized beads for 60 minutes. Next, cells were washed and stained for CD3 A700 (BD, cat. 557943), CD14 APC-Cy7 (BD, cat. 557831, clone MφP9), CD66b Pacific Blue (Biolegend, cat. 305112, clone G10F5), and fixed in 4% PFA. Neutrophils were defined as SSC-high, CD66b+, CD3-, CD14-, CD11c-. The degree of phagocytosis was measured by flow cytometry on a BD LSR II flow cytometer (for gating strategy see Figure S4) and a phagocytic score was calculated as in the ADCP assay. Each IgG sample was tested on fresh cells from two individual healthy donors, and a geometric mean score was calculated.

Antibody-dependent cellular cytotoxicity (ADCC) assay

The rapid fluorescent ADCC (RF-ADCC) assay was performed as described previously (Gómez-Román et al., 2006). In brief, CEM-NKr cells (Aids reagent, cat. 4376) were pulsed with recombinant HIV gp120 (sf162) and labeled with CFSE and the membrane dye PKH26. NK cells were enriched directly from seronegative whole blood donors by negative selection using RosetteSep (Stem Cell Technologies). Purified IgG was added to the labeled, antigen-pulsed CEM-NKr cells. Next, fresh NK cells were added, prior to a 4hour incubation at 37°C. Cell were fixed before acquired on a BD LSR II flow cytometer (for gating strategy see Figure S4), and the proportion of cells that maintained membrane expression of PKH26 but lost CFSE staining was determined.

Antibody-dependent complement deposition (ADCD)

CEM cells were pulsed with recombinant HIV gp120 (sf162) and incubated with purified IgG from individual donors. Fifteen ul of freshly isolated, HIV negative donor plasma, diluted 1:10 with veronal buffer and 0.1% gelatin, was added before incubation for 20 minutes at 37°C. Cells were then washed with 15 mM EDTA in PBS, and complement deposition was detected via flow cytometry (for gating strategy see Figure S4) following staining for C3b-FITC on the surface of cells (Cedarlane, cat. CL7632F; Clone: 10C7).

Antibody-dependent NK cell activation

Ab-dependent NK cell degranulation and cytokine/chemokine secretion was measured as previously described (Chung et al., 2014) with minor modifications. Briefly, CEM-NKr cells were pulsed with recombinant HIV gp120 (sf162). Fresh NK cells were isolated from whole blood from seronegative donors using negative selection with RosetteSep (StemCell). The antigen-pulsed CEM-NKr cells and isolated primary NK cells were mixed and purified Abs, anti-CD107a (BD, cat. 555802), brefeldin A (10 mg/ml) (Sigma), and GolgiStop (BD) were added before incubation for 5 hours at 37°C. The cells were then washed and stained for surface markers using anti- CD16 (BD, cat. 557758), anti-CD56 (BD, cat. 557747), and anti-CD3. The cells were then washed, fixed and permeabilized using Fix & Perm (Invitrogen), and then stained intracellularly with anti-IFN-γ (BD, cat. 554702) and anti- MIP-1β (BD, cat. 550078). The cells were then fixed in 4% paraformaldehyde and analyzed on a BD LSR II flow cytometer (for gating strategy see Figure S4).

Luminex Isotype Assay

A luminex assay was used to quantify the relative concentration of each antibody isotype among the HIV-specific antibodies as previously described. Briefly, Luminex microplex carboxylated beads (Luminex) were coupled to recombinant HIV gp120 (sf162) via covalent NHS-ester linkages by combining EDC and NHS (Thermo Scientific) in PBS. The coupled beads (2500 beads/well) were added to a 96-well filter plate (Millipore). Donor plasma was added and incubated at 4°C overnight. The beads were washed three times with 100 μL of PBS-Tween, and incubated with individual IgG isotype detection reagents (total IgG, IgG1, IgG2, IgG3, and IgG4) conjugated to PE (Southern Biotech). The 96-well plate was incubated, with shaking, for 2 hours (500 rpm), washed four times, and read on a Bio-Plex 3D Suspension Array System (Bio-Rad).

Glycan analysis of anti-HIV-specific IgG

HIV-specific antibodies were purified and Fc- antibody glycosylation was analyzed by capillary electrophoresis, as previously described (Mahan et al., 2016; Mahan et al., 2015). Briefly, plasma samples were passed over gp120 (sf162) embedded columns. The bound antibodies were eluted, treated with Ides, and the Fc portion isolated. Glycans were released using enzymatic digestion with Peptide-N-Glycosidase F (PNGaseF, New England Biolabs). Glycans were labeled with 8- aminopyrene-1,3,6-trisulfonic acid, excessive dye removed before resuspended in ultrapure water. Glycans were analyzed on a 3500 XL sequencer (Applied Biosystems). Area under the curve for each peak was calculated as a fraction of total glycan composition. For Glycan subgroup designations see Table S1.

B cell sorting

PBMCs were stained, following thawing, with live dead, CD3, CD14, CD19, CD21, CD27, CD38, and CD138, to track the overall changes in B cell phenotypes. The overall expansion of live/CD3-CD14-CD19+/−CD138+ cells was monitored to ensure that a significant plasmablast expansion was observed across 3 vaccinees. Low levels of plasmablasts were observed at baseline, with a 5-19 fold increase following vaccination. Single CD19+CD27+ B cells were sorted, to capture both memory and plasmablast populations into RLT buffer followed by whole transcriptome amplification using a modified SMART-Seq2 protocol. Libraries were prepared using a Nextera XT Sample Preparation Kit and samples were then sequenced on an Illumina NextSeq 500 using 250-bp paired-end reads. The sequencing data was first demultiplexed to separate multiplexed single cell samples using index sequences that were attached to the template during library preparation. The raw sequence reads were checked using FastQC for sequence data quality control. Spliced Transcripts Alignment to a Reference (STAR) software was used to reduce mapping error rates and to enhance mapping speed with flexibility in alignment. Quality control criteria were considered to remove low quality cell transcripts. Only the single cells that had a 1) total number of reads > 1 million, 2) percentage of reads mapping to known exons > 50%, 3) a minimum of > 6000 genes detected, 4) < 15% of reads mapping to mitochondrial genes and 5) < 20% of reads mapping to ribosomal genes. RSEM software (Li and Dewey, 2011) was used to quantitatively estimate gene abundance from the aligned sequence reads. For normalization of single-cell RNA-seq data, pooled library size factor (Scran) (Lun et al., 2016), following by remove unwanted variation (RUV) (Risso et al., 2014) was calculated to adjust for nuisance technical effects. The overall level of B4Galt3 gene expression was selectively analyzed across all sorted cells. The single-cell RNA-seq analysis pipline was implemented in a customized script in python and ran on the High-performance Linux server cluster.

B cell flow cytometry, HIV DNA and usHIV RNA for the PNB cohort

Please see methods and data available in original publications (Olesen et al., 2015; Rasmussen et al., 2014).

QUANTIFICATION AND STATISTICAL ANALYSIS

Construction of correlation network

Networks were constructed based on the correlations between antibody glycan profiles and functional profiles at each sampling time point as well as relative changes from baseline (v1) to capture dynamics during PNB treatment using Gephi. The edges represent significant positive (rho > 0) correlations between any given two nodes with an adjusted *p-value* correcting for multiple hypothesis testing (False discovery rate adjusted p value < 0.05). In addition, the edge weights between nodes were determined by the correlation coefficient (rho). To remove visual noise, intra-functional and intra-glycan correlations were removed.

Identification of the viral rebound specific correlates with Elastic-Net/PLSR

The minimal set of antibody features and functional parameters that collectively associated to viral rebound dynamics (DNA and days to rebound) was defined by using Elastic Net regularization (Zou and Hastie, 2005), followed by partial least-squares regression (PLSR). Elastic Net regularization was used to reduce the number of the features and to select the features most relevant to the outcome. The alpha (α) in Elastic Net optimization, controlling the weight of L1 norm and L2 norm, was determined by 5-fold cross validation given the whole dataset. After feature selection, PLSR was used to define the relationship between the input as a linear combination of the selected features and the outcome (viral rebound time or viral reservoir). Specifically, PLSR seeks the latent variables, which linearly combine the features, which explain the maxim variance of the outcome. As results, this approach produced a model that generates the greatest separation among the antibodies from low to high outcome with the lowest possible mean squared error (MSE). Prior to Elastic-Net/PLSR analysis, the data was normalized with mean centering and variance scaling. In order to generate a robust PLSR model less sensitive to the outliers, a bootstrap framework for Elastic-Net/PLSR analysis was applied, which contained 5000 repetitions of 5-fold cross validation (Cawley and Talbot, 2010). In each repetition, the dataset was randomly divided into 5 folds, where 4-fold of the dataset was used for Elastic-net/PLSR model optimization (inner cross-validation) and the remaining holdout set was used to test the model (outer cross-validation). Ultimately, each feature was weighted by the frequency of being selected among 5000 cycles and was ranked by the weights. To determine the minimal set of the correlates, we applied a sequential step-forward approach where the algorithm started with the best feature and, for each step, the next best feature was added into the PLSR model. The model prediction performance in each step was evaluated by MSE calculated from 5-fold cross-validation, and the set of the features showing the lowest MSE was defined as the minimal set of the correlates. Finally, variable importance in projection (VIP) along with the final model was calculated, a weighted sum of squares of the PLS weights, which summarized the importance of the features in a PLSR model (Galindo-Prieto et al., 2014). To estimate statistical significance of the correlation (R^2), the correlation of the predicted and the observed outcome, two types of random permutation tests (Verbyla and Litvaitis, 1989) were computed, 1) outcome shuffling, shuffling the order of the outcome labels. 2) size-matched random feature selection, randomly selecting the features in the same size as the actual minimal set of the correlates. In total 10,000 random models from each of both tests were collected to estimate the null distributions for the R^2. Eventually, an empirical, nominal p value for the R^2 in each test was calculated relative to this null distribution, which represents the statistical significance of the prediction results by the true model compared to the random models. The whole computational modeling pipeline was implemented in a customized script in MATLAB (Mathworks, Natick, MA).

Additional statistical methods

Basic statistical analyses were performed using Prism software, version 6.0 for Mac (GraphPad Software). Wilcoxon signed rank test was used for longitudinal comparisons between baseline (v1) and later time points (v6, v9 or v12). Spearman's rank method was used to test for correlation. A p value less than or equal to 0.05 was considered significant. False discovery rate (FDR)- adjusted p values were calculated by the method of Benjamini–Hochberg. Statistical methods of the Elastic Net / PLSR model is described in detail above. For each figure, the designated statistical method is described in the corresponding figure legends.

Author/s:
Offersen, R; Yu, W-H; Scully, EP; Julg, B; Euler, Z; Sadanand, S; Garcia-Dominguez, D; Zheng, L; Rasmussen, TA; Jennewein, MF; Linde, C; Sassic, J; Lofano, G; Vigano, S; Stephenson, KE; Fischinger, S; Suscovich, TJ; Lichterfeld, M; Lauffenburger, D; Rosenberg, ES; Allen, T; Altfeld, M; Charles, RC; Ostergaard, L; Tolstrup, M; Barouch, DH; Sogaard, OS; Alter, G

Title:
HIV Antibody Fc N-Linked Glycosylation Is Associated with Viral Rebound

Date:
2020-12-15

Citation:
Offersen, R., Yu, W. -H., Scully, E. P., Julg, B., Euler, Z., Sadanand, S., Garcia-Dominguez, D., Zheng, L., Rasmussen, T. A., Jennewein, M. F., Linde, C., Sassic, J., Lofano, G., Vigano, S., Stephenson, K. E., Fischinger, S., Suscovich, T. J., Lichterfeld, M., Lauffenburger, D. ,... Alter, G. (2020). HIV Antibody Fc N-Linked Glycosylation Is Associated with Viral Rebound. CELL REPORTS, 33 (11), https://doi.org/10.1016/j.celrep.2020.108502.

Persistent Link:
http://hdl.handle.net/11343/273766

File Description:
Published version